Enhancing Synthetic Rating Curve Development Through Empirical Roughness Built for Hydrofabric Datasets

J. Michael Johnson[1,2,3], Damilola Eyelade[1,2,3], Justin Singh-Mohudpur[1,2,3], Arash Modaresi Rad[1,3], James Coll[1, 3], Ryan Spies[1,3], Lilit Yeghiazarian[4]

[1] Lynker, Fort Collins Colorado USA.

[2] Department of Geography, University of California, Santa Barbara, California, USA.

[3] NOAA NWS Office of Water Prediction

[4]University of Cincinnati

Corresponding author: J Michael Johnson (jjohnson@lynker.com)

Key Points:

- We established synthetic rating curves (SRC) at 7,270 gaged locations and calibrated roughness to minimize error in predicted streamflow.
- A predictive model based on hydrofabric network properties was built to estimate roughness to support SRC creation in ungauged basins.
- These predictions achieved a correlation of 0.89 but are likely dependent on the resolution of the DEM and hydrofabric used.

Abstract

Rating curves are commonly developed through direct observation, open channel flow models, or mechanical methods, each relying on in-situ measurement. As part of a U.S. effort to provide high resolution, continental scale, flood mapping, synthetic rating curves (SRCs) were developed across the National Hydrography Dataset (NHDPlusV2) to translate flows, like those generated by the NOAA National Water Model, into river depths. This approach uses Digital Elevation Models (DEM) to define the necessary cross-sectional properties for Manning's equation. A significant limitation, alongside an opportunity for broad improvement, has been assigning suitable roughness without local information. We applied the DEM based methodology to generate SRCs at 7,270 locations with known USGS rating curves, and calibrated roughness to minimize the error between predicted and observed flow. Subsequently, we tested several approaches based on land cover, stream order, and the hydrographic network to estimate the optimized values in a manner that can be extended to ungauged catchments. Among these, a predictive Machine Learning (ML) model based on the NHDPlusV2 network attributes demonstrated superior ability to estimate the optimized roughness with a Spearman correlation of 0.89. Sensitivity analysis showed improving accuracy of DEM and roughness is crucial for accurate estimation of the lower and mid/upper parts of SRC, respectively. Finally, we applied the predictive model over the NHDPlusV2, generating reach-level roughness estimates that can directly support national flood mapping efforts. The method is generalizable to any hydrofabric network that contains topology; however the generated values are dependent on the DEM and hydrofabric used.

Plain Language Summary

Synthetic rating curves (SRCs) have been developed for every river segment in the United States as part of the Continental Flood Inundation Mapping Framework (CFIM). A mathematical equation called the Manning's equation and a Digital Elevation Model (DEM) map are the baseline requirements for creating these SRCs. Studies have shown that with careful estimation of roughness, these SRCs can be used to create detailed, real-time flood maps when paired with streamflow simulations like those from the NOAA National Water Model. Normally, channel roughness is estimated from field surveys, model calibration, or tables that ask about the channel and its surroundings. However, in practice, this approach is limited to surveyed locations. Here we used the DEM based SRC methodology to generate SRCs at 7,270 locations with known USGS rating curves. From these we identified the best roughness value that would minimize the error between predicted and observed flow. We tested several approaches for predicting these values including using land cover, stream order, and hydrographic properties of the National Hydrography Dataset (NHDPlusV2). The latter proved most capable at predicting roughness and was applied over the ~2.7 million NHDPlusV2 reaches.

1 Introduction

Stage-discharge relationships are pivotal in flood mapping and routing, providing essential insights into river behavior during flood events (Guerrero et al., 2012; Guven & Aytek, 2009). Manning roughness coefficients, which signify channel and floodplain resistance to flow, are integral to refining these relationships (Mansanarez et al., 2019). Accurate estimation of Manning roughness is particularly crucial in ungagged locations, where streamflow data is scarce

(Karamouz & Mahani, 2021). By employing empirical relationships, remote sensing data, or land use analysis, hydrologists can estimate Manning roughness coefficients for such areas, improving flood mapping and routing accuracy (Zheng et al., 2018). This enhanced precision aids in better understanding flood dynamics and facilitates more effective flood risk management, ultimately reducing socio-economic impacts associated with floods.

Stage-discharge relationships depend on the hydraulic characteristics of the stream channel, are known to vary over time, and are subject to numerous sources of uncertainty, including unstable control, non-uniform flow, and local stage variability (A. Hamilton & Moore, 2012; S. Hamilton, 2008; McMahon & Peel, 2019; Muste et al., 2012; Westerberg et al., 2011). A rating curve represents a relationship between two variables, most commonly discharge (Q) and an elevation relative to a datum, more commonly referred to as stage (m). While there are many approaches for establishing rating curves, they broadly include empirical (direct and indirect measurements), mechanical, and theoretical methods. *Direct empirical methods* require streamflow measurements following an approach developed in the 1890s (Kean & Smith, 2005; Rojas et al., 2020). However, obtaining measurements can pose challenges particularly during high flow events and maintenance requires considerable resources leading to an increasing number of defunded gauges (Kean & Smith, 2005). *Indirect empirical methods* employ a variety of flow models that require measured channel geometry, specified water surface elevations, and an empirical roughness value to characterize resistance to flow (Benson & Dalrymple, 1967). Roughness is known to vary with stage and is typically calibrated for a specific set of flow rates (Barnes, 1967; Jarrett, 1984; Kubrak et al., 2019; Limerinos, 1970; Marcus et al., 1992). However, since resistance cannot be assigned without prior knowledge, indirect methods have limited ability to generate complete, stage-discharge relationships (Kean & Smith, 2005). Furthermore, even when calibrated, empirical roughness only captures friction, or skin resistance, while neglecting drag generated by the normal forces acting on a water volume (Kean & Smith, 2005). As a result, *mechanical models* have been used to estimate drag and friction explicitly using in-situ measurements of channel geometry, as well as the physical roughness of the bed, banks, floodplain, and vegetation density (Kean & Smith, 2005). These models have been shown to provide more accurate discharge estimates at a lower cost than many indirect methods (Kean & Smith, 2005, 2010).

While observations, empirical, and mechanical methods are ideal, the requirement for on-site measurements limit their application at large scales. Assigning roughness values represents one of the most challenging processes to generalize and is one of the most sensitive parameters in streamflow calculations (Hutton et al., 2012). To provide continental flood forecasts (J Michael Johnson et al., 2019; J. Michael Johnson, Narock, et al., 2022; Maidment, 2016), and enhanced emergency response (Dallo et al., 2020; J Michael Johnson et al., 2018), Zheng et al. (2017) proposed a method to estimate reach-level synthetic ratings curves (SRC) from Digital Elevations Models (DEM) as part of the National Flood Interoperability Experiment (NFIE; Maidment, 2016). This theoretical rating curve method estimates the hydraulic characteristics from a Height Above Nearest Drainage (HAND) raster (Nobre et al., 2011; Rennó et al., 2008) and the National Hydrography Dataset (NHDPlusV2, McKay et al., 2012), making the method extendable to ungauged basins. In the first iteration of the NFIE, and in the following Continental Flood Inundation Mapping framework (CFIM), a default global roughness of 0.05 was used. (Zheng et al., 2017) found a global roughness for SRCs resulted in variable accuracy, but also that accurate depth estimates could be achieved for the studied Tar River Watershed by calibrating roughness to a stage-discharge relation produced from HEC-RAS modeling. (Zheng

et al., 2018) implemented the HAND approach using a LIDAR DEM, calling the approach 'GeoFlood', finding it capable of capturing the Federal Emergency Management Agency (FEMA) flood plain coverage with 60–90% accuracy when adjusting the roughness to best align the SRC to a measured United States Geological Survey (USGS) rating curve. As part of that study, the authors highlighted an extreme sensitivity to even small variations in roughness. Other studies have carried out indirect evaluations of the skill of SRCs by comparing HAND-based inundation maps to remotely sensed flood products and aerial imagery in which the assignment of roughness was identified as a principal limiting factor in accurate flood prediction (Garousi-Nejad et al., 2019; J Michael Johnson et al., 2019). Today, the CFIM approach is actively being developed as an open-source flood inundation mapping software (FIM) operated and maintained by the National Oceanic and Atmospheric Administration's (NOAA) National Weather Service (NWS) (NOAA-OWP, 2021, p.). In FIM3, a stream order-based roughness is applied to move beyond *default global roughness* values. A study by (Qi & Liu, 2019) demonstrated the importance of considering land-use changes and its significant impact on alteration of roughness coefficient that results in drastic changes in estimated extreme flood peaks.

Collectively, this emerging body of evidence recognizes that improved estimates of roughness are crucial for the success of the continental flood mapping framework. The objective of this work is to estimate a national set of reach-level empirical roughness values suitable for theoretical rating curves to enhance operational flood prediction and other hydroscience calculations reliant on estimated roughness. We propose a novel approach for more accurate estimation of roughness using a Machine Learning (ML) model trained on NHDPlusV2 network attributes and compare our results to widely accepted methods for estimating roughness in both academic literature and operational settings. By calculating the explicit spatial representation of roughness within the context of national scale FIM efforts, we directly address many of the shortcomings associated with the static parameterization of roughness, enabling us to more concretely isolate the various sources of error within the SRC. In the *data* section, we outline the datasets used. In the *methods* section, we describe the existing SRC calculation techniques; the methods used to optimize roughness to USGS rating curves, and to estimate roughness based on stream order, land cover, and the hydrofabric network. Lastly, we introduce performance metrics for evaluating model skill. The *discussion* examines SRC performance using the different roughness estimates; how different sections of the rating curves exhibit error; and the sensitivity of SRC generation to the input DEM, hydrofabric, and selected roughness. Finally, the conclusions highlight the implications of this work as well as the limitations of the provided data and opportunities for the continued use of the broader approach.

2 Data

2.1 Observed USGS Rating Curves

The USGS measures rating curves on a 6–8-weeks schedule and disseminates the information Water Information System (NWIS: https://waterdata.usgs.gov/nwis/sw) (Beran & Piasecki, 2008; De Cicco et al., 2018). A sample of 7,270 active USGS rating curves were collected from NWIS, and recorded stage values were converted to depths by subtracting the reported zero-flow stage from all stage values. Normalizing depths to the zero-flow record allows us to estimate the local reference datum by assuming the zero-flow is referenced to the surveyor-defined channel bottom.

For each rating curve, a natural cubic spline was fitted and used to estimate stage values for 25 evenly spaced intervals ranging from 0 to the maximum observed streamflow. Observed USGS rating curves are subject to random gage measurement errors and systematic errors resulting from cross section changes, scouring, bed fill and backwater effects (McMillan & Westerberg, 2015). However, we assume these relationships to be accurate at the scale of a continental study, and our goal is to approximate these recorded relationships. Future work can build on extensive studies like those carried out in Australia (McMahon & Peel, 2019) to characterize the uncertainty in the observed ratings.

2.2 Hydrofabric Data

The medium-resolution National Hydrography Dataset Version 2 (NHDPlusV2: 1:100,000 scale) digitally mapped the surface water network of the continental United States (CONUS) into ~2.7 million river segments with similar hydrologic characteristics (McKay et al., 2012) NHDPlusV2 comprises the original NHD Flowline geometries, the 30-meter National Elevation Dataset, and "value-added attributes" (VAA's) that encompass pre-calculated network characteristics enhancing network analysis. While VAAs are precomputed for NHDPlusV2, they can be generated for any set of hydrofabric data with a topology (D. Blodgett et al., 2020, 2023; D. L. Blodgett & Johnson, 2022a). In this research, we aggregated VAA analysis attributes into single file, accessible as a HydroShare resource (J M Johnson, 2021). Methods for accessing the tabular VAA table were incorporated into the USGS nhdplusTools R package (D. L. Blodgett & Johnson, 2022b) to support this research. By segregating attribute data from geometry, we can more readily use this information in statistical and ML models. In future iterations of hydrofabric whether it be MERIT (Yamazaki et al., 2019), TDX-hydro (McCormack et al., 2022), the USGS/NOAA Reference Fabric (Bock et al., 2022), or the NOAA Next Generation Water Resource Modeling Framework hydrofabric (J. Michael Johnson, 2022), simular characteristics can be computed.

2.3 Height Above Nearest Drainage Data

The Height Above Nearest Drainage (HAND) is a normalized elevation dataset that describes the height of each cell above the nearest designated flow path (Nobre et al., 2011). In 2018, (Y. Y. Liu et al., 2018) generated a HAND dataset for the Continental United States (CONUS) using the 10-meter USGS National Elevation Dataset (NED), the NHDPlusV2, and the D∞ distance down calculation available in TauDEM (Tesfa et al., 2011). All HAND data, along with intermediate processing steps, are accessible on the University of Texas (UT) Corral server (https://web.corral.tacc.utexas.edu/nfiedata/). This dataset has been updated as part of the Continental Flood Inundation Mapping (CFIM) framework implemented at Oak Ridge National Laboratory (Y. Y. Liu et al., 2020) and was used in this research.

3 Methods

We employed the DEM-based SRC methodology to generate and validate roughness values based on their capacity to replicate streamflow-depth relationships akin to recorded USGS rating curves. In this section, we outline the process of establishing reach level hydraulic properties (3.1), estimating roughness (3.2), comparing SRCs to observed values (3.3), and evaluating the sensitivity of the input parameters (3.4).

3.1 Estimation of Reach Average Hydraulic Properties

Manning's equation (equation 1) characterizes open channel flow as a function of channel velocity, flow area, slope, and roughness (Chow, 1959; Farmer et al., 2019; Pavelsky, 2014). Originally developed for uniform flow conditions where the water-surface profile and energy gradient are parallel to the streambed, and the cross-sectional area, hydraulic radius, and depth remain constant throughout the reach. It can be assumed that equation 1 is equally valid for the nonuniform reaches typically found in floodplains (Jarrett, 1984).

$$Q(y) = \frac{A(y) \times R(y)^{\frac{2}{3}} \times \sqrt{S}}{n} \quad (1)$$

where:

Q(y) = the discharge at depth y (m^3/s),
A(y) = the cross-sectional area at depth y (m^2)
R(y) = the hydraulic radius at depth y (m)
S = the longitudinal slope (m/m)
n = the Manning's roughness coefficient

The method proposed by Zheng, Tarboton et al. (2018) calculates cross-sectional area (A), hydraulic radius (R) and streambed slope (S) from HAND, the hydrofabric information. It necessitates a user-defined roughness as illustrated in Figure 1. This iterative process is replicated for a predetermined set of stage (Y) values.

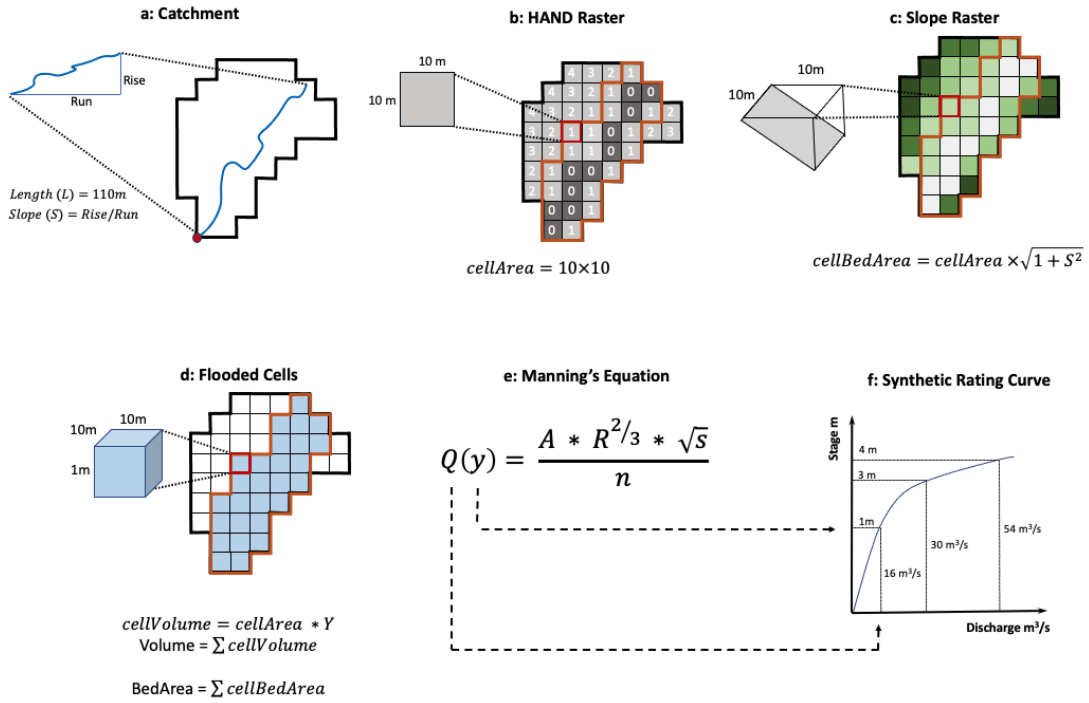

Figure 1: Process for creating stage-discharge relationships as defined in Zheng, Tarboton, et al., (2018). (a) The catchment boundary establishes contributing cells, and the flowpath length (L) and slope (S) are then defined by the hydrofabric. (b) The HAND raster stores the elevation above the nearest river cell in the contributing area. (c) The slope raster defines the effective bed surface area of each cell dependent on the raster resolution. (d) For a defined stage (e.g., Y=2), inundated cells (outlined in orange across panels) are determined as those where HAND ≤ Y. The volume and bed area of the inundated cells are then computed from (b) and (c). (e) Manning's Equation estimates a flow rate Q. (f) A collection of Y-Q relations defines an SRC.

As illustrated in Figure 1a, possible contributing cells (all those that are "nearest a drainage") are selected, in this case using the NHDPlusV2 catchment. The NHDPlus VAA attributes provide the stream length (L; m) and longitudinal slope (S; m/m), and the HAND raster provides the elevation difference between each grid cell and the nearest flow path. A slope raster (1c) contains the percent slope (cellSlope) of each grid cell, which can be used to estimate the effective ground surface or bed area (BA) at a given depth (Equation 2).

$$BA = cellres^2 \sqrt{1 + cellslope^2} \quad (2)$$

For any defined stage (Y; meters), the HAND raster can be used to identify inundated cells where the HAND value is less than Y (1d). At each of these cells, a water volume (V) can be calculated as the depth of ponded water multiplied by the cell area (Equation 3).

$$V(y) = cellres^2 \times (Y - HAND) \quad (3)$$

For all inundated cells, the total bed area (∑BA) and volume (∑V(y)) can approximate the cross-sectional area (Equation 4), wetted perimeter (Equation 5), and hydraulic radius (Equation 6) needed in Manning's Equation (Figure 1e).

where:

$$A(y) = \sum \frac{V(y)}{L} \quad (4)$$

$$WP(y) = \sum \frac{BA(y)}{L} \quad (5)$$

$$R(y) = \frac{A(y)}{WP(y)} \quad (6)$$

Iterating this calculation over a defined set of depths using a defined single value or stage-varying roughness yields a streamflow-depth table resembling a rating curve (Figure 1f).

3.2 Estimating the Roughness Terms

In various hydrology subfields, roughness is often estimated based on stream order or land cover characteristics. Models such as WRF-Hydro assign roughness as a function of Strahler stream order for overland flow calculation and Muskingum-Cunge hydrograph routing (Gochis et al., 2016a). In 2016, Li introduced the NHDPlus Inundation Modeler V4.0, which relies on a separate stream order-based approach (Li, 2016). In both lumped and distributed hydrologic models, land cover datasets are frequently used to assign roughness through

reclassification tables, with similar methodologies applied in dam breach analysis and other 2D hydrologic and hydraulic models (Janssen, 2016; Kalyanapu et al., 2009; Z. Liu et al., 2019).

Furthermore studies have demonstrated that a stage-varying composite roughness (*N*), based on defined in-channel and overbank regions may outperform a single roughness value (Boulomytis et al., 2017; Kubrak et al., 2019; Nguyen & Fenton, 2005). The composite approach has been shown to reduce error in hydraulic models by as much as 70% for surveyed reaches (Tuozzolo et al., 2019). Although there are multiple ways to define a composite roughness, (Tullis, 2012) found Horton's equation (Equation 7: Chow, 1959) to yield the most consistent results across disparate channel types.

$$N = \frac{(P_{ch}(n_1)^{1.5} + P_{ob}(n_2)^{1.5})^{\frac{2}{3}}}{P_{total}^{\frac{2}{3}}} \quad (7)$$

Where:

N = composite roughness value,

n_1 = in-channel *n*

n_2 = overbank *n*

P_{ch} = wetted channel perimeter (m)

P_{ob} = wetted overbank perimeter (m)

P_{total} = total wetted perimeter (m).

In locations where a USGS rating curve is available, we can determine an optimized roughness by minimizing the error between observed and simulated flows. In locations without a known rating curve, we can build on prior methodologies and assign single value and composite roughness values based on stream order or land cover. Additionally, we introduce a ML approach that leverages the VAAs of the hydrographic network to estimate roughness based on patterns found in the optimization exercise. Within these approaches, multiple variants are tested, resulting in eleven unique methods that are described below.

3.2.1 Optimization

Optimized roughness values aim to minimize the error between simulated and observed discharge for given depths. By fitting the roughness term alone, it is assumed (tested in 3.4) that uncertainty in other inputs (DEM and hydrofabric) are minimal. To define a single roughness for each NHDPlusV2 catchment, we solved equation 1 using a nonlinear least squares regression model (NLS) based on the Gauss-Newton algorithm with 50 maximum iterations, a convergence tolerance of 1e-09, a lower bound of 0.01, an upper bound of 0.40, and an initial guess of 0.05 (J. M. Johnson et al., 2024; J. Michael Johnson, Coll, et al., 2022). Considering the DEM and hydrofabric data as static, the roughness value (n) is the only term in Manning's equation that can be adjusted via calibration . The lower and upper bounds were selected based on literature-driven values for reasonable floodplain roughness, with the initial guess derived from the CFIM precedent. In all cases, the NLS solver converged, and varying the initial guess had no discernible impact on the estimation in a sample of 500 basins.

A composite roughness was defined for each catchment by treating all cells with a HAND value of 0 as in-channel, and the remaining as out-of-channel. Both n_1 and n_2 were

estimated using a NLS model with bounds of (0.01 and 0.20), and (0.01 and 0.40), respectively, with an initial guess of 0.05 for each. A final constraint ensured that n_1 was less than n_2 in each solution. Multiple starting values were tested in a selected subset of basins with no notable differences in the results. Combined, the single value and composite optimized results provide a validation dataset used throughout this research.

3.2.2 Stream Order-Based Estimation

Previous studies (Cosgrove et al., 2020; Gochis et al., 2016b; Li, 2016) have used stream order as a proxy for roughness. We aim to evaluate how these approximation tables compare to the mean and median single value optimized derived from the USGS rating curves. Table 2 presents these values alongside those used in Li (2016) and the WRF-Hydro/National Water Model version 2.0 RouteLink file. In the National Water Model implementation of WRF-Hydro, both an in-channel roughness (*n*) and a compound channel roughness (nCC) are associated with each flowline feature of NHDPlus.

Table 1. Roughness values used for the Stream order approximations

Order	Mean Optimized	Median Optimized	Li-Assignment	WRF-Hydro n	WRF-Hydro nCC
Source			*Li (2016)*	*Gochis (2016)*	*Gochis (2016)*
1	0.196	0.187	0.14	0.060	0.12
2	0.181	0.169	0.12	0.060	0.12
3	0.157	0.134	0.09	0.055	0.11
4	0.128	0.103	0.09	0.055	0.11
5	0.107	0.079	0.07	0.050	0.10
6	0.088	0.057	0.06	0.050	0.10
7	0.083	0.051	0.03	0.045	0.09
8	0.067	0.043	0.03	0.045	0.09
9	0.047	0.029	0.03	0.040	0.08
10	0.043	0.037	0.03	0.040	0.08

3.2.3 Land Cover Estimation

Land cover information can provide a spatially heterogeneous perspective of the landscape, yet it is prone to sampling and resampling error as well as scale-related classification uncertainties (J Michael Johnson & Clarke, 2021; Kim et al., 2024). Foster and Maxwell (2019) identified that vegetation-defined heterogeneity influenced behavior and determined n values in the stream network, but grid resolution did not reveal a clear scaling relationship. Hence, we are interested in both single flood plain values, akin to those used in flood mapping studies, and stage-varying roughness values.

The 2019 National Land Cover Database (NLCD) underwent reclassification using roughness values proposed by Kalyanapu et al. (2009) and extended by Liu et al. (2019). A single floodplain roughness was calculated for each reach by averaging all cells submerged by the maximum stage in the rating curve. Furthermore, a stage-varying roughness was generated by calculating the average land cover roughness using only the inundated cells at each stage.

3.2.4 Hydrofabric Gradient Boosted Machines (GBM)

Roughness is dependent on a variety of channel characteristics, making it a suitable candidate for exploration with predictive ML models. After evaluating multiple options, a Gradient Boosted Machine (GBM) algorithm was selected. GBMs are known to enhance model generalizability (Friedman, 2001)but due to lack of inherent regularization, and highly complex decision boundaries they tend to focus on difficult-to-fit data points and result in overfitting. However, adjusting its hyperparameters and applying early stopping can mitigate this issue. In contrast to supervised single predictive models or those based on ensemble averages (e.g., random forests), GBMs sequentially add new models to an ensemble and update a trained base learner with each iteration.

Fitting GBMs necessitates several hyperparameters, including the number of trees (T); an interaction depth (K); a learning rate (**λ**); and subsampling controls (p). The interaction depth (K) determines the number of splits in each tree and the pace at which the algorithm proceeds down the gradient descent. Smaller learning rates (**λ**) reduce the likelihood of overfitting but prolong the convergence time. While these parameters confer flexibility to GBM models, they demand intensive tuning to select appropriate values. Hence, a grid of potential hyperparameters for this problem was defined as follows (Equation 8):

$$hyperparameters = \begin{Bmatrix} \mathrm{k} = 1,2,\dots,15 \\ \mathrm{T} = 500, 1000, \dots, 5000 \dots\ 10000, 15000, \dots, 40000 \\ \lambda = 0.001, 0.005, 0.01, \dots, 0.1 \\ \mathrm{R} = 5, 10, 15 \\ \mathrm{p} = 0.3 \end{Bmatrix} \quad (8)$$

To identify the variables that most accurately predict roughness, we defined a training dataset using a stratified random sampling method, selecting 500 or 80% of the gauged locations from each HUC2 from the Watershed Boundary Dataset. Developing a GBM approach involves a three-step process.

Step 1:

Initially, a series of 16,065 GBMs were fitted for each hyperparameter combination (Equation 8), using all numeric variables from the NHDPlusV2 VAA as predictors. For each model, the relative influence of each predictor was computed in addition to the number of times it was selected for splitting, weighted by the squared improvement provided at each split. These results were averaged over all trees (Friedman, 2001), and those with the highest relative influence were paired with a subjective evaluation of how easily they could be computed for general hydrofabric networks, yielding the final set of 5 core predictors:

i. **Drainage Area**: Drainage area (km^2) of the single flowpath catchment
ii. **Flowpath Length**: Flowline length in kilometers
iii. **Arbolate Sum**: The cumulative length of the upstream drainage network (mainstem and tributaries) from the outlet of the catchment
iv. **Path Length**: The distance from the flowline outlet to the end of the network along the mainstem path
v. **Slope**: A unitless fraction (cm/cm) of the flow path slope derived from the 30m NED

Step 2:

Using only these five predictors, a new set of 16,065 GBMs was trained for all hyperparameter combinations, and the combination producing the minimal RMSE was selected to train a final model. That model used the following:

i. k = 12
ii. T = 40,000
iii. $\lambda = 0.025$
iv. R = 10
v. p =0.3

Upon completion, the predicted roughness values generated with this model had an RMSE of 0.045, and a nRMSE of 26.4%, when compared to the single value optimized roughness values.

Step 3:

Using the model trained in step 2, we predicted roughness across the NHDPlusV2 network. Similarly, any river segment with a known drainage area, flowpath length, arbolate sum, path length, and slope can serve as input to develop a predicted single value roughness. It is critical to note that the predicted values are unique to the input NHDPlusV2 dataset; extrapolation or conflation to a different network would likely provide poor results. Nonetheless, new data can be generated from the model provided a network topology is known

3.3 Synthetic Rating Curve Comparison

This optimized roughness (*n*), a standard default value (0.05), a stream order based, land cover based, and GBM approaches produce eleven synthetic (and one observed) rating curve at each of the 7, 270 gauged locations. For clarity, these methods are summarized in Table 2.

Table 2: Methods and approaches for assigning roughness for rating curves

#	Category	Name	Description
1	observed	USGS	25 evenly distributed Q-Y points built from a cubic spline fit to the observed USGS rating curve
2	default	global-roughness	Roughness of 0.05 assigned to all reaches
3	optimized	single-value	Single roughness, fit to the observed rating curve using a non-linear solver with a lower and upper bound of 0.01 and 0.4.
4	optimized	composite	Composite roughness using Horton's method where n_1 and n_2 were fit to the observed rating curve using a non-linear solver with a lower and upper bound of {0.01, 0.01} and {0.2, 0.4}.
5	stream order	Li-assignment	Roughness assigned by stream order based on Li, 2016
6	stream order	wrf-N	Roughness assigned by stream order from the 'Manning's roughness' (*n*) in the NWM v2.1 RouteLink file
7	stream order	wrf-Ncc	Roughness assigned by stream order from the 'Compound Channel Manning's *n*' (*nCC*) in the NWM v2.0 RouteLink file
8	stream order	mean-optimized	Roughness assigned by stream order based on mean values from the calibrated method
9	stream order	median-optimized	Roughness assigned by stream order based on median values from the calibrated method

10	land cover	single-value	Single value assigned via a reclassified land cover map using those values submerged by maximum RC stage
11	land cover	stage-varying	Stage varying values assigned via a reclassified land cover map using cells submerged by the current RC stage
12	hydrofabric	GBM	Values assigned based on output of trained GBM model using the NHDPlus VAA attributes as predictor variables

To assess SRC accuracy, the simulated discharge values produced with each roughness, using the USGS rating curve stage values, were compared to the USGS discharge values using the root mean squared error normalized to the mean of observed discharge (nRMSE; see Equation 9).

$$nRMSE = 100 \times \sqrt{\frac{\overline{(Q_{src} - Q_{obs})^2}}{\overline{Q_{obs}}}} \quad (9)$$

where:

Q_{obs} = observed discharge

Q_{src} = simulated discharge.

nRMSE was calculated for the entire rating curve as well as the lower, middle, and upper sections. While defining "good" and "bad" nRMSE is subjective, a cut off of 30% nRMSE has been used to determine whether a site displays reasonable performance in prior research (Gleason & Smith, 2014; Yoon et al., 2016). For readability throughout the text, we adopt this shorthand and describe errors of 30% or less as reasonable, and errors of 100% or more as extreme.

3.4 Parameter Sensitivity

One open question about SRCs is how sensitive the results are to input data including the DEM, hydrofabric, and roughness. To decompose the SRC into its primary components, Manning's Equation can be rewritten by substituting equations 4, 5, 6 into equation 1, and rearranging such that:

$$Q(y) = V \times \frac{1}{n} \times \frac{1}{L} \times \sqrt{S} \quad (10)$$

Where

$$V = \frac{Vol(y)^{\frac{5}{3}}}{BA(y)^{\frac{2}{3}}}$$

To understand the role of each of the input dataset in streamflow estimation, we want to perform sensitivity analyses with respect to the four uncertain parameters - V, *n*, L, and S - by implementing a separate sensitivity analysis at stages 1, 2, 3 … 25 using a factorial design.

To build the factorial design for sensitivity analysis, we need to establish reasonable range bands for each of these variables that are adjustable to each site. The volume factors are driven by the DEM which is most easily influenced by the vertical accuracy as highlighted in case studies leveraging LIDAR (Zheng et al., 2018). The 10m NED has a documented vertical accuracy of 3.04 meters (Gesch et al., 2014) so we elected a test set of 0.5, 1 and 2 meters in the

positive and negative directions basin wide. These were implemented by adjusting the HAND values throughout a given catchment prior to estimating volume and bed area.

To test roughness, we allow roughness to range from 0%, 10%, 25%, 50%, 100% and 200% error from the optimized single-value estimates while enforcing the lower and upper limits of 0.01 and 0.40. Length is a byproduct of the hydrofabric resolution and higher resolution data inputs like the NHD High-Resolution will likely increase reach length as more detail is captured. Following research aligning multi-scalar flowline data from the EPA River Reach, Medium Resolution NHDPlus and High Resolution NHD through the identification of common mainstems (D. Blodgett et al., 2020), a high-level comparison revealed a range of variability which we reduced to 0%, 5%, 10% and 15% percent of the NHDPlusV2 flowline values in the positive and negative direction.

Slope is a product of the hydrofabric and underlying DEM. While the HAND and Slope rasters are based on the 10m NED, the NHDPlus flowline slope is an attribute derived from the 30m NED. A random sample of 100 flowlines from this study were used to extract transects from the 10m NED. The difference between the smoothed slopes of these transects (5 point rolling mean) and the listed slope attributes of the NHDPlus were represented as a 0%, 25%, 50% and 75% error in each direction of the recorded values.

Using these possible variations, 363 randomly sampled sites were evaluated to ensure accuracy at the 95% confidence level. The results of the design were analyzed with an Analysis of Variance (ANOVA) method to deduce the main effects and two factor interactions using the *multisensi* R package (Bidot et al., 2018). Upon completion, the results were averaged across locations.

4 Results

A total of 81,070 synthetic rating curves (SRCs) were computed for comparison. Section 4.1 describes the performance of each roughness method, section 4.2 addresses errors exhibited in each section of the rating curve, section 4.3 addresses the skill of the GBM model, and section 4.4 looks at the sensitivity of the SRCs to the roughness, DEM, and hydrofabric inputs used in Manning's equation.

4.1 Synthetic Rating Curve Performance Analysis

Figure 2A illustrates the percentage of locations achieving reasonable and extreme error for each roughness method, alongside the Spearman Correlation compared to the optimized single value roughness. In the outlined section of the table, the 25^{th}, 50^{th}, and 75^{th} quartile (Q1, Q2, Q3) nRMSE for the complete rating curve, and the mean nRMSE for each section of the rating curve are displayed. These statistics are derived solely from sites producing nRMSE < 100% for that method.

The two optimized approaches provide the least error across all metrics but are confined to gaged locations. SRCs generated with an optimized composite roughness offer marginal improvement over those with an optimized single value, and occasionally exhibit degraded performance. This implies that a composite view, particularly when considering locations where HAND = 0 as in channel, is not critical to SRC roughness estimation. The optimized single value approach achieved reasonable error in ~80% of the tested locations, suggesting models potential accuracy across a broad spectrum of locations. Nonetheless, the remaining 20% highlight areas where the HAND-based SRC model may be incomplete or other sources of uncertainty contribute to the error.

476 Amongst methods extendable to ungaged basins, the GBM method demonstrates superior
477 results and notably reduced error compared to stream order and land cover approaches. Notably,
478 it generates nearly four times as many SRCs with reasonable error as other nonsite optimized
479 methods. The correlation with the optimized single value is also double compared to the next
480 closest method.
481 All four stream order methods exhibit similar performance metrics and offer marginal
482 improvement over the global default. Stream order information primarily reduces the number of
483 sites with extreme error (nRMSE > 100%). This is done best by the mean optimized stream order
484 values. This performance improvement over a global default value emphasizes that roughness is
485 a local phenomenon, and the thematic assignment is too generalized to provide significant
486 performance gains. The two land cover methods demonstrate identical performance, with neither
487 land cover method offering an improvement over the stream order methods, and added
488 substantial computational burden.
489 Finally, a default global roughness of 0.05 achieves nRMSE ≤30% in just 10% of the
490 locations emphasizing the need for a spatially heterogeneous approach and the value in seeking a
491 more sophisticated approach. To visualize these statistical patterns spatially, Figure 2B maps the
492 nRMSE from the best performing method for each approach. While the magnitudes of error in
493 the optimized and GBM methods differ, the maps highlight regions of the country where large
494 errors persist across all methods. Prominent examples include the gulf coast of Florida, the
495 eastern seaboard, the Atlanta metro region, and to a lesser extent, the lower Mississippi
496 floodplain.
497

A. Evaulation Metrics

Method	Approach	nRMSE ≤30%	nRMSE >100%	Correlation with Optimized	Q1 nRMSE	Q2 nRMSE	Q3 nRMSE	mean nRMSE lower	mean nRMSE middle	mean nRMSE upper
Single Value	Optimized	78.10	8.81	1.00	6.14	11.88	21.58	40.22	15.79	11.73
Composite N	Optimized	76.74	10.32	NA	4.62	10.54	20.86	37.12	15.16	11.20
GBM	Hydrographic	61.85	16.21	0.88	7.46	14.76	31.38	44.70	22.40	18.61
Median Optimized	Stream Order	16.10	40.37	0.44	28.53	49.13	71.63	58.11	44.18	42.39
Mean Optimized	Stream Order	15.74	35.21	0.43	30.65	52.60	74.27	60.15	46.35	44.33
Li Assignment	Stream Order	15.09	46.29	0.41	27.74	48.10	72.06	57.90	43.83	42.08
wrf-nCC	Stream Order	14.59	40.51	0.40	30.42	51.80	73.52	59.93	46.03	43.88
wrf-n	Stream Order	12.15	59.52	0.40	25.95	46.53	73.16	56.60	43.06	42.09
Single Value	Land cover	11.50	34.74	-0.05	38.00	63.57	82.95	64.98	52.66	51.15
Stage-Varying	Land cover	11.32	34.66	NA	38.01	63.53	82.74	64.52	52.42	51.20
Global roughness	Default	11.28	61.32	NA	26.60	48.09	73.87	57.20	43.52	42.56

B. Mapping nRMSE

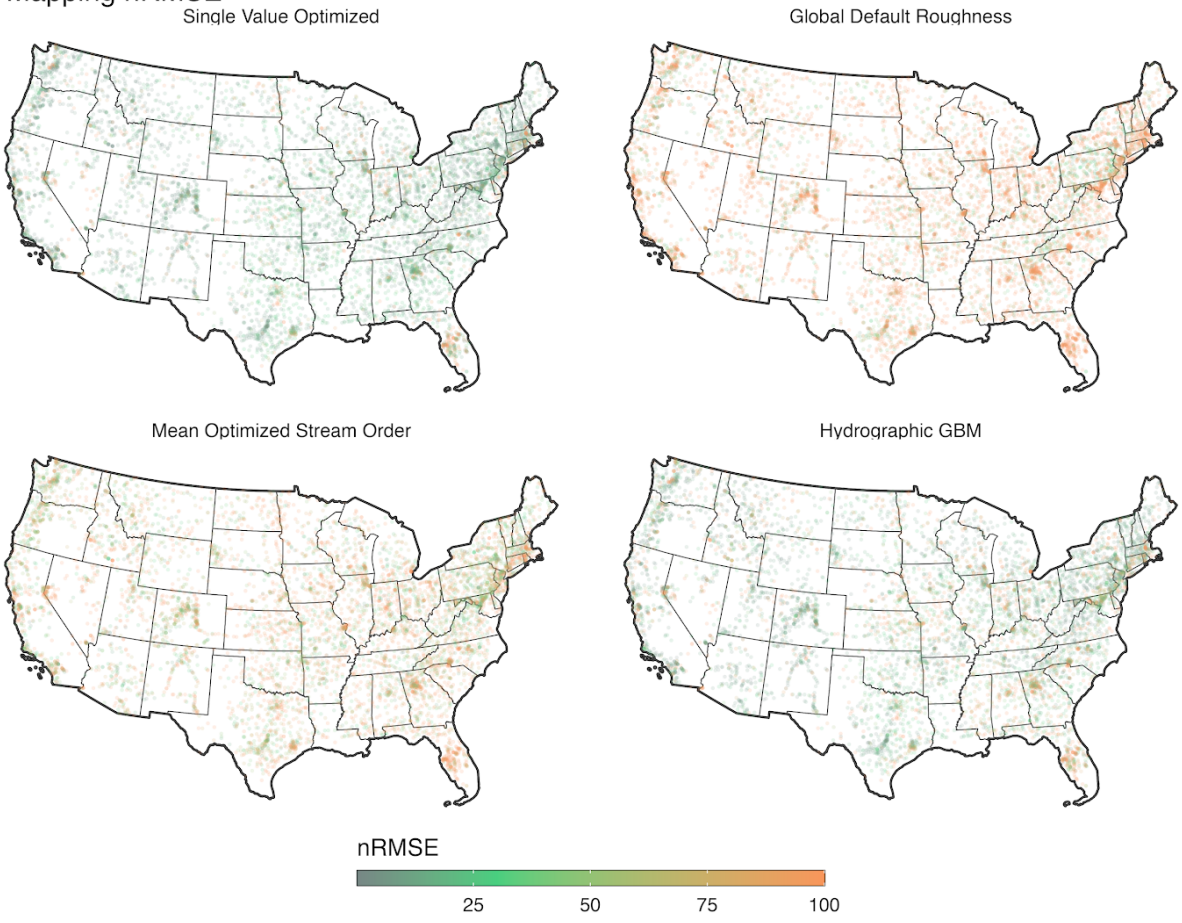

Figure 2: (**a**) Synthetic rating curve accuracy across methods. Quartile error values and the percentage of sites with reasonable and extreme errors are listed. The methods are sorted by the Q2 criteria, and darker hues represent better performance and are applied column-wise. (**b**) The nRMSE from each method is mapped.

Across all methods, there is consistently more error in the lower section of the rating curve compared to the middle and upper portions. SRCs developed with a global default and mean optimized stream order have the highest mean nRMSE across all sections of the curve. The

single value optimized and hydrofabric GBM approaches both reduce the mean nRMSE in each section; however, the error remains higher by a factor of 2+ in the lower third. This pattern may have to do with (1) lack of bathymetric representation in HAND data for in-channel flows, (2) the datum adjustment applied to achieve a zero-flow USGS rating curve, or (3) that at smaller flows/depths, small errors are more impactful than the errors at higher flows/depths. Nonetheless, estimated SRCs demonstrate greater accuracy at the higher end of the rating curve, which holds promise for flood mapping studies and other use cases. Moreover, this staggered performance suggests the potential to optimize *n* for various sections of the rating curve based on flow which could be provided by the National Water Model. While a composite *n* was not found to be a valuable addition, a stage-varying *n* might offer improvements.

4.2 Model and Optimized Skill

The error for the single-value optimized method provides the best possible result given the current DEM, hydrofabric, and roughness bounded to the range of {0.01, 0.4}. Taking the DEM and hydrofabric data as static, the only term in Manning's equation that can be calibrated is the roughness value. The roughness value serves as a proxy for representing the ratio of water volume to discharge. Very large n values represent situations where a very strong resistance to flow is used to reduce discharge when HAND volumes are large for a given stage, but the actual SRC derived discharge is low. Very low values of n represent the opposite situation where calculated water volumes based on HAND properties are low but the required discharge is quite large. This observation may suggest a need to represent channel bathymetry to accommodate excess HAND water volumes. This section focuses on comparisons between the single optimized value and GBM approaches, particularly the cases where the imposed lower and upper limits were reached – likely to address issues in other inputs to Manning's equation.

The error for the single-value optimized method provides the best possible result given the current DEM, hydrofabric, and roughness bounded to the range of {0.01, 0.4. Figure 3A shows the difference in roughness between the optimized and GBM approach. Sites with an absolute value of $\Delta N < 0.01$ have been removed from the map. In this Figure, sites that appear red indicate that the N value of the GBM based on network attributes is greater than the optimized n value; conversely, sites that are blue indicate the opposite. On the East coast, we observe a landscape where the GBM tends to show greater roughness compared to the optimized values while in the southeast, the GBM tends to show lower N. The rest of the country indicates a more mixed approach, with a slight tendency for the GBM to predict n lower than the optimized approach (blue).

Next, we categorized the *skill* of the rating curve (by the nRMSE < 30% threshold) and whether the roughness pushed toward the upper limit (>0.35), the lower limit (<0.05), or was within a fair range ($0.05 \leq n \leq 0.35$). In total, this yielded six categories that were used to classify the GBM and optimized-based SRCs. Figure 3B shows the confusion matrix of these divided into four color-coded quadrants while Figure 3C shows categorical classification. The first column (green and orange box) represents the total number of sites that were well-served by the site-by-site optimization. In total, 77.9% of the locations achieved reasonable error, and 54.2% did so without stretching the roughness value toward the imposed limits. For those that did push roughness towards an imposed limit, the bulk stretched towards the low value. This highlights the tendency of the GBM model to favor lower roughness and a broader notion that HAND volumes tend to under-predict the actual volume flowing through the river channel. The first row (green and black box) represents the total number of sites that were well-served by the GBM

552 model. In total, 62.1% of the sites were able to achieve reasonable error, with ~15% stretching
553 the roughness value toward the imposed limits.
554 Starting in the upper left, the green section shows that 62.1% of sites achieve a
555 reasonable nRMSE in both the single-value optimization and GBM. 46.8% of these did so with
556 an in-range roughness, while ~15% pushed the upper and lower limits. Specifically, there is a
557 strong preference to push the optimization roughness towards the lower limit of 0.01.Moving
558 counterclockwise, the black box is empty, highlighting that the GBM cannot find solutions
559 where the optimization failed. The red box represents situations where both the optimization and
560 GBM methods were unable to find a solution. The implicit concern is that the errors in the input
561 data are larger than what roughness adjustments alone can correct in ~22% of the tested
562 locations.
563 In total, 17.8% of sites produced bad optimizations with the same pattern for both site-
564 based optimized and GBM methods. For example if a site had a bad nRMSE with a low n, the
565 GBM produced the same which is encouraging for the skill of the GBM, but suggests future
566 work might look to eliminate these sites in the model training. In the remaining 4.2% percent, the
567 GBM took on a low or high optimized n, and brought it into the expected range without
568 improving the performance.

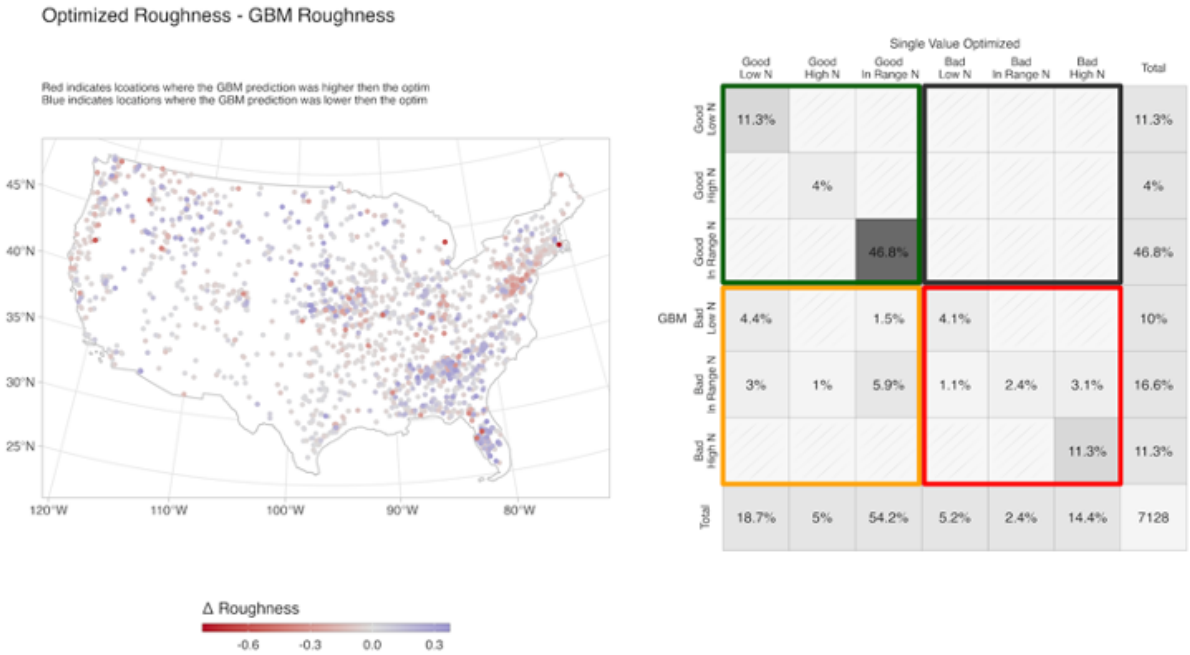

Percent of sites per stream order that fall into each classification

Single Site Optimized Approach

	Order 1	Order 2	Order 3	Order 4	Order 5	Order 6	Order 7	Order 8	Order 9	Order 10
Good High N	6.8	8.8	8.6	5.4	3.4	2.6	3.0	0.0	0	0
Bad High N	56.8	33.3	17.2	9.7	6.5	4.8	5.7	6.0	4	0
Good Low N	2.4	3.9	8.6	16.2	25.8	35.6	38.3	40.5	40	50
Bad Low N	0.5	1.3	1.3	3.4	7.6	10.6	10.5	21.4	24	0
Good In Range N	31.2	50.5	61.1	62.6	54.2	44.2	39.2	31.0	28	50
Bad In Range N	2.4	2.2	3.2	2.7	2.5	2.1	3.3	1.2	4	0

Figure 3: (**a**) The difference in roughness produced by the GBM and Optimized roughness values are mapped. Red (negative values) indicate locations where the GBM prediction produces higher values than the optimized approach. Blue (positive values) indicate locations where the GBM prediction produces roughness lower than the optimized approach. Sites where the difference was less the +-.01 where excluded (**b**) The GBM and single site optimized results were categorized by the skill of the rating curve (by the nRMSE < 30% threshold), and whether the roughness pushed toward the upper limit (>0.35), the lower limit (<0.05), or was within the range ($0.05 \leq N \leq 0.35$). **(c)** The percent of sites, per stream order, that fall into each classification. Darker hues represent larger percentages. The horizontal line after order 4 represented a break in SRC creation performance identified in prior research.

4.3 Parameter Sensitivity

In this section we investigate the sensitivity of SRCs to the primary inputs using factorial design and ANOVA decomposition, which include the (1) DEM, (2) hydrofabric, and (3)

583 roughness. Figure 4 shows the sensitivity indices of the main effects and first-order interactions
584 at each point in the rating curve normalized to 1.

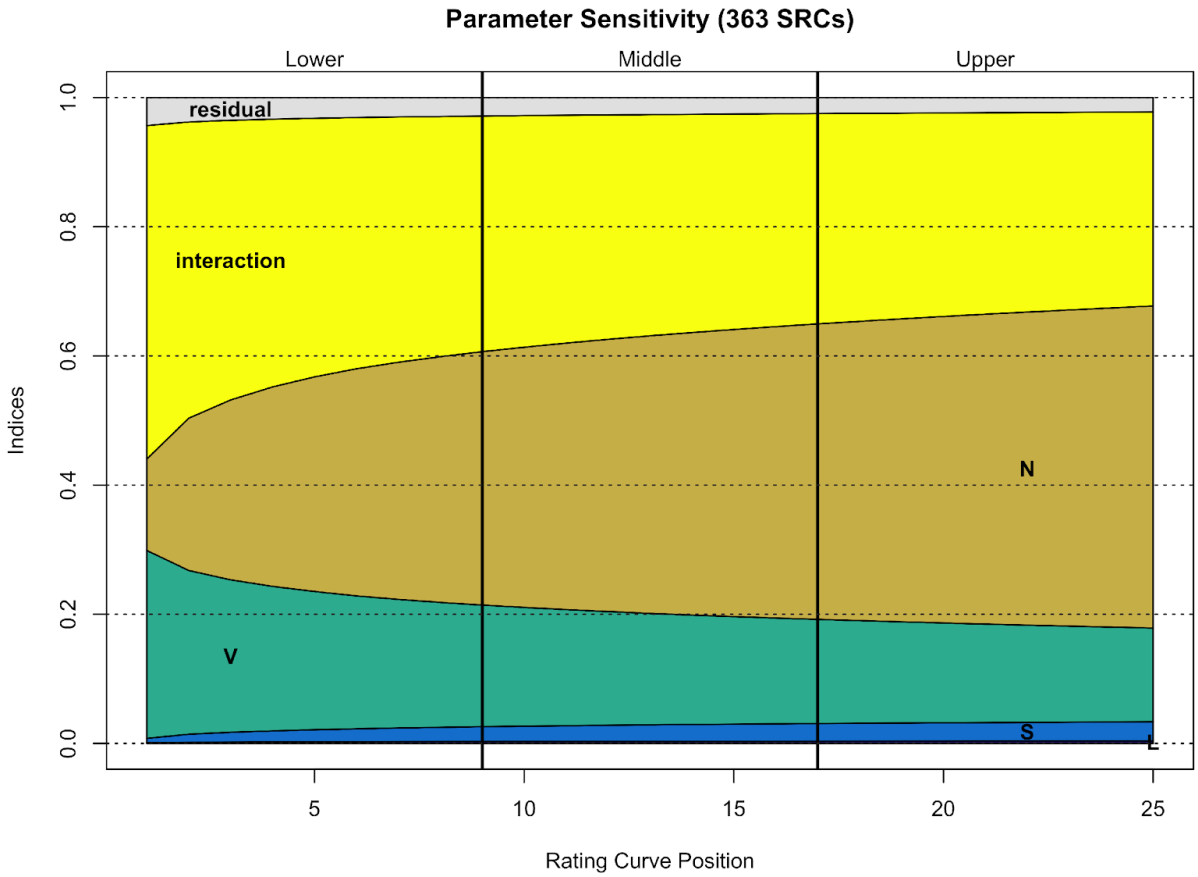

585
586 **Figure 4**: Evolution of the main effects and the first-order interaction sensitivity indices of the SRC
587 variables averaged over 363 randomly selected locations.

588 In the lower third of the rating curve, there is more sensitivity to the DEM (*V*), interaction terms,
589 and residual effects. This suggests that SRCs perform worse in the lower third of the rating curve
590 largely because they are more easily influenced by multiple factors. Starting around the middle
591 of the rating curve, proportional sensitivity starts to stabilize with ~15% being contributed by the
592 DEM, ~45% by roughness, and ~30% from variable interaction. There is minimal error (in total
593 ~10%) contributed from the length, slope, or residual effects of the model combined. It is notable
594 that as one approaches the upper end of the curve, the contribution of error from the interaction
595 and *V* terms decrease further and are generally overtaken by sensitivity to roughness.
596 These results indicate that the primary challenge in developing accurate SRCs is
597 Manning's roughness for mid and high SRC values, and very low SRCs are affected by DEM
598 errors and missing bathymetry, but there are other key sources of uncertainty. The overwhelming
599 sensitivity to roughness means that areas suffering from other inputs can only be identified when
600 the uncertainty in roughness is minimized. Given that the primary objective of many operational
601 flood inundation forecasting systems is to warn of high magnitude events, optimization of
602 roughness for this objective seems practical. For those seeking predictive skill for lower

magnitude events, i.e., “nuisance” flooding, improving accuracy of base information such as the DEM seems to be more critical.

Aside from roughness and the interaction of all inputs, the volume of water computed from the DEM was the largest source of error. As the USGS 3D elevation program moves their elevation program towards the collection of nationally comprehensive and complete LIDAR coverage, it is worth mentioning here the possible opportunities and limitations with the method provided here.

5 Discussion

A challenging aspect of the transferability of our proposed methodology is the scale-dependency of both DEM that plays a crucial role in generating water volume for a given depth defined by a HAND product, and hydrographic properties that are used for roughness calculations. Ideally we would like the trained roughness ML model to be transferable to any other hydrographic network generated at different scales. We conjecture that this holds true for networks of comparable scale (i.e., 1:100,000 ratio). Another question is whether the assumption that the variable selected during the feature importance analysis remains consistent as hydrographic network scale changes? For instance in higher resolution networks, characterized by the prevalence of more tributaries with greater sinuosity, the arbolate sum, a key characteristic, typically demonstrates a notable increase. Consequently, if a smaller river system within the higher resolution network is trained solely on lower resolution data, it might erroneously exhibit attributes akin to those of a much larger system, potentially resulting in artificially low roughness values.

Similar to hydrographic scale impact on roughness, the higher resolution LiDAR or DEM data improves accuracy in channel volume estimation and synthetic rating curve calculation by providing detailed terrain data, enhancing channel morphology representation, and minimizing uncertainties in channel geometry and hydraulic modeling. This contributes to more reliable assessments of water resources and flood risks. The utilization of LiDAR data holds promise for mitigating uncertainty in volume estimations through several mechanisms. The first method, akin to that employed in GeoFlood, involves increasing the horizontal (grid) resolution to yield more effective "cells." This reduction in resampling inherently enhances the vertical accuracy at each cell. The second method entails utilizing LiDAR to refine vertical accuracy within the same 10m grid as the current 3DEP 10m product, effectively integrating the latest data captures to enhance the existing grid. In both scenarios, if a new DEM is utilized, recalibration of the base inputs to a Synthetic Rating Curve (SRC) – namely, the cross-sectional area and hydraulic radius at depth Y – following the methodology outlined by Zheng et al. (2017) is necessary. This entails updating the GBM model based on the full hyperparameter set (Step 2) but does not necessitate retraining on the complete set of VAA attributes (Step 1).

Despite the potential enhancements to the current DEM, the issue of changing scales (cell resolution) raises an open question. To qualitatively assess the transferability of GBM-produced roughness values across DEM scales, we compared the reported, tuned roughness values at five USGS sites examined in Zheng et al. (2018) to the GBM values. While the GBM approach tended to overpredict roughness compared to the reported GeoFlood values, a correlation was observed (albeit from a limited dataset). This trend aligns with the notion that larger grid cells yield larger volumes and, per equation 11, necessitate larger roughness values. The idea that roughness varies with DEM resolution finds support in hydrologic modeling research. For example, it has been established that 2D flood models are sensitive to DEM resolution (Fewtrell

et al., 2008; Horritt & Bates, 2002; Saksena & Merwade, 2015; Schumann et al., 2007), and roughness (Lim et al., 2016; Mason et al., 2003; Pappenberger et al., 2005). However, conflicting findings exist regarding the existence of a scaling relationship, with some studies suggesting otherwise (M. Foster & M. Maxwell, 2019). Hence, it is acknowledged that the dependency of GBM roughness values on DEM and hydrography constitutes a limitation of the dataset produced herein, not the methodology. Future investigations will explore methods for operationalizing roughness model fitting and prediction based on the methods and data (USGS rating curves) developed in this study.

An assessment of the sites exhibiting extreme error in SRC with the calibrated n values demonstrated that SRC extreme error often occurs when roughness approaches one of the enforced physical limits. It was also in these areas where the largest divergence between the predicted and calibrated n values was observed. In many ways, this divergence in n values offers a signal for when other aspects of the SRC creation are uncharacteristically influential. The value of n serves as a proxy for representing the ratio of water volume to discharge. Very large n values represent situations where a very strong resistance to flow is used to reduce discharge when HAND volumes are large for a given stage, but the actual SRC derived discharge is low. Very low values of n represent the opposite situation where calculated water volumes based on HAND properties are low but the required discharge is quite large. (perhaps suggesting a need for representing channel bathymetry to accommodate excess HAND water volumes).

Finally, several critical considerations arise when utilizing this dataset or extending the workflow beyond its current scope. The workflow, beginning with a mechanical measurement of roughness to train a predictive model based on network attributes, subsequently utilized the same network and DEM to establish a relationship between water surface height and discharge required for that stage. However, the applicability of these findings to variations in input parameters, such as alterations to the underlying network, remains unclear. Further inquiry is warranted to determine whether the values derived from this dataset could be used as a direct crosswalk to the new network, whether the values would need to be recalculated based on the new attributes of the network using the existing model, whether the model would need retraining using the new inputs, or whether the process of determining the selected features needs to be performed.

6 Conclusions

At the onset of this research, the necessity for improved reach-level roughness was highlighted to support continental flood mapping efforts. We employed the methodology proposed by Zheng et al. (2017) to define reach-averaged hydraulic traits from a 10m HAND product in catchments with a USGS gauge and calibrated a roughness value to minimize the error in predicted flows. This approach resulted in 78% of gaged locations achieving nRMSE ≤ 30%. To produce SRCs in ungauged basins, we evaluated a range of methods for estimating reach-level roughness. Among these, a data-driven ML model based on NHDPlus hydrographic topology proved the most robust. The ML model produced almost four times the number of SRCs with acceptable error compared to non-optimizable methods (e.g., stream order and land cover methods). Additionally, its correlation with the optimized single value is twice that of the next closest method. The predictions were able to achieve a ranked correlation of 0.89 with the optimized values and SRCs with reasonable error in 62% of the tested locations. In contrast, a widely used global roughness value captured just 13% of SRCs with reasonable error, and the best performing stream order parameterization captured just 16%.

A sensitivity test showed that the DEM and roughness are the principal sources of error in the conceptual rating curve model, while length and slope are practically non-significant. We demonstrated that as the upper end of the SRC is approached, it becomes apparent that the contribution of error from the interaction and V terms decrease further and are generally overtaken by sensitivity of roughness. These conclusions are generally in line with other work that has looked at HAND-based SRC uncertainty at individual sites (Godbout et al., 2019). The conclusion is that in locations where roughness is the primary contributor of uncertainty, the data driven roughness and existing data inputs can produce reasonable SRCs. In areas where the DEM and hydrography introduce uncertainty, the calibrated values take on a role that was not *per se* roughness, but rather a broad error-reducing scalar. Such locations were not pervasive, and generally clustered around regions with large built-up extents, known engineered controls, or low relief. In these areas where DEM fidelity is a primary source of SRC error, there is capacity for LIDAR to be used with the methods suggested as part of the GeoFlood project (Zheng et al., 2018). A drawback to using LIDAR is the availability, procurement costs, and computational needs associated with creating HAND and generating inundation forecasts at large scales. Fortunately, the 10m DEM seems serviceable for the majority of CONUS, and the SRC error map (Figure 2) can help prioritize areas where the integration of LIDAR data might be especially beneficial.

Future work will involve exploring several avenues to address key findings in this research and potential implications. Firstly, we demonstrated a disparity in error across different sections of the rating curve, particularly higher error in the lower section compared to the middle and upper portions. This signals a need to evaluate the absence of bathymetry in the model, as the missing channel volume likely impacts the lower end of the rating curve. Secondly, the findings suggest promising prospects for FIM methods that rely on Synthetic Rating Curves (SRCs) for high flow applications. Thirdly, there is potential for optimizing the roughness coefficient (n) for various sections of the rating curve. While a composite n was not found to be beneficial, a stage-varying n might prove advantageous. Lastly, future research will explore how this method scales across different networks, assessing its applicability and performance in diverse hydrological settings. Within the United States, LIDAR may provide better discretization and some additional bathymetry data. The effects of this can be tested at reaches that have both LIDAR and USGS rating curves. These datasets can be effective in training a ML model and gaining a better understanding of the effect of grid cells and data driven roughness on model training. In essence, further research may be able to quantify how more location-attuned roughness values can contribute to improved large-scale hydrologic routing and other applications of reach-level roughness.

For regions outside the USA, official stream network data similar to the NHD are few and far between. Publicly available data are often aggregated at lower spatial resolutions, decreasing the ability to represent the full drainage network. However, the rapid increase in the amount of crowd-sourced stream network data available through platforms like OpenStreetMap offers the promise of high-resolution data that can be used for improved global reach level modeling for smaller rivers. Localized high-resolution official drainage networks, crowd-sourced stream network data offer the opportunity to evaluate the impact of scale, network density, and attributes on the ability of GBM models to characterize the rating curve relationship. Overall, the value of the current work lies in the data produced for the scale of the medium-resolution NHD and 10m 3DEP product, as well as a method and curated set of training data to apply to other scales within and outside the United States. The roughness values have been made publicly

available on HydroShare with easy-access options for both R and Python. With respect to R, the roughness values can be accessed with the nhdplusTools *get_vaa* functionalities. We hope the use of this data can support improved flood forecasting, applications that need to estimate roughness, and can prompt consideration of what other hydrologic properties and characteristics can be learned and supported by the topology implicit to hydrography datasets.

Acknowledgments

Parts of writing this work were performed with funding from the National Science Foundation's Urban Flooding Open Knowledge Network Center (Grants 1937099, 2033607). Any opinions, findings, and conclusions or recommendations expressed in this material are those of the authors and do not reflect the views of the National Science Foundation.

Disclaimer

The views expressed in this article do not necessarily represent the views of NOAA or the United States.

Open Research

The roughness values generated in the research are available at (J M Johnson, 2021). The GBM model is available at https://github.com/LynkerIntel/hydrofabricML. A version of this software will be published through Zenodo after the review process to accommodate for any needed changes.

References

Barnes, H. H. (1967). *Roughness characteristics of natural channels*. US Government Printing Office.

Benson, M. A., & Dalrymple, T. (1967). *General field and office procedures for indirect discharge measurements*. US Govt. Print. Off.,.

Beran, B., & Piasecki, M. (2008). Availability and coverage of hydrologic data in the US geological survey National Water Information System (NWIS) and US Environmental Protection Agency Storage and Retrieval System (STORET). *Earth Science Informatics*, *1*(3–4), 119–129.

Bidot, C., Lamboni, M., & Monod, H. (2018). Multisensi: Multivariate sensitivity analysis. *R Package Version*, *2*, 1–1.

Blodgett, D., Johnson, J. M., Sondheim, M., Wieczorek, M., & Frazier, N. (2020). Mainstems: A logical data model implementing mainstem and drainage basin feature types based on WaterML2 Part 3: HY_Features concepts. *Environmental Modelling & Software*, 104927.

Blodgett, D., Johnson, J. M., & Bock, A. (2023). Generating a reference flow network with improved connectivity to support durable data integration and reproducibility in the coterminous US. *Environmental Modelling & Software*, *165*, 105726.

Blodgett, D. L., & Johnson, J. M. (2022a). Hydrologic modeling and river corridor applications of HY_Features concepts. Retrieved from http://www.opengis.net/doc/PER/22-040

Blodgett, D. L., & Johnson, J. M. (2022b). nhdplusTools: Tools for Accessing and Working with the NHDPlus.

Bock, A., Blodgett, D. L., Johnson, J. M., Santiago, M, & Wieczorek, M.E. (2022). *National Hydrologic Geospatial Fabric Reference and Derived Hydrofabrics: U.S. Geological Survey data release*. Retrieved from https://doi.org/10.5066/P9NFPB5S

Boulomytis, V. T. G., Zuffo, A. C., Dalfré Filho, J. G., & Imteaz, M. A. (2017). Estimation and calibration of Manning's roughness coefficients for ungauged watersheds on coastal floodplains. *International Journal of River Basin Management*, *15*(2), 199–206.

Chow, V. T. (1959). Open-channel hydraulics. *McGraw-Hill Civil Engineering Series*.

Cosgrove, B. A., Gochis, D. J., Clark, E. P., & Flowers, T. (2020, January 13). NOAA's National Water Model: A Dynamically Evolving Operational Hydrologic Forecasting Framework. American Meteorological Society. Retrieved from https://ams.confex.com/ams/2020Annual/webprogram/Paper365698.html

Dallo, I., Stauffacher, M., & Marti, M. (2020). What defines the success of maps and additional information on a multi-hazard platform? *International Journal of Disaster Risk Reduction*, *49*, 101761.

De Cicco, L. A., Lorenz, D., Hirsch, R. M., Watkins, W., & Johnson, M. (2018). *dataRetrieval: R packages for discovering and retrieving water data available from U.S. federal hydrologic web services* (manual). Reston, VA: U.S. Geological Survey / U.S. Geological Survey. https://doi.org/10.5066/P9X4L3GE

Farmer, W. H., LaFontaine, J. H., & Hay, L. E. (2019). Calibration of the US geological survey national hydrologic model in ungauged basins using statistical at-site streamflow simulations. *Journal of Hydrologic Engineering*, *24*(11), 04019049.

Fewtrell, T., Bates, P. D., Horritt, M., & Hunter, N. (2008). Evaluating the effect of scale in flood inundation modelling in urban environments. *Hydrological Processes: An International Journal*, *22*(26), 5107–5118.

Friedman, J. H. (2001). Greedy function approximation: a gradient boosting machine. *Annals of Statistics*, 1189–1232.

Garousi-Nejad, I., Tarboton, D. G., Aboutalebi, M., & Torres-Rua, A. F. (2019). Terrain Analysis Enhancements to the Height Above Nearest Drainage Flood Inundation Mapping Method. *Water Resources Research*, *55*(10), 7983–8009. https://doi.org/10.1029/2019WR024837

Gesch, D. B., Oimoen, M. J., & Evans, G. A. (2014). *Accuracy assessment of the US Geological Survey National Elevation Dataset, and comparison with other large-area elevation datasets: SRTM and ASTER* (No. 2331–1258). US Geological Survey.

Gleason, C. J., & Smith, L. C. (2014). Toward global mapping of river discharge using satellite images and at-many-stations hydraulic geometry. *Proceedings of the National Academy of Sciences*, *111*(13), 4788–4791.

Gochis, D., Dugger, A., McCreight, J., Karsten, L. R., Logan, Yu, W., et al. (2016a). *Technical Description of the National Water Model Implementation of WRF-Hydro*.

Gochis, D., Dugger, A., McCreight, J., Karsten, L. R., Logan, Yu, W., et al. (2016b). *Technical Description of the National Water Model Implementation of WRF-Hydro*.

Godbout, L., Zheng, J. Y., Dey, S., Eyelade, D., Maidment, D., & Passalacqua, P. (2019). Error assessment for height above the nearest drainage inundation mapping. *JAWRA Journal of the American Water Resources Association*, *55*(4), 952–963.

Guerrero, J.-L., Westerberg, I. K., Halldin, S., Xu, C.-Y., & Lundin, L.-C. (2012). Temporal variability in stage–discharge relationships. *Journal of Hydrology*, *446*, 90–102.

Guven, A., & Aytek, A. (2009). New Approach for Stage–Discharge Relationship: Gene-Expression Programming. *Journal of Hydrologic Engineering*, *14*(8), 812–820. https://doi.org/10.1061/(ASCE)HE.1943-5584.0000044

Hamilton, A., & Moore, R. (2012). Quantifying Uncertainty in Streamflow Records. *Canadian Water Resources Journal/Revue Canadienne Des Ressources Hydriques*, *37*(1), 3–21.

Hamilton, S. (2008). Sources of uncertainty in Canadian low flow hydrometric data. *Canadian Water Resources Journal*, *33*(2), 125–136.

Horritt, M., & Bates, P. (2002). Evaluation of 1D and 2D numerical models for predicting river flood inundation. *Journal of Hydrology*, *268*(1–4), 87–99.

Hutton, C. J., Brazier, R. E., Nicholas, A. P., & Nearing, M. (2012). On the effects of improved cross-section representation in one-dimensional flow routing models applied to ephemeral rivers. *Water Resources Research*, *48*(4), 2011WR011298. https://doi.org/10.1029/2011WR011298

Janssen, C. (2016). Manning's n Values for Various Land Covers To Use for Dam Breach Analyses by NRCS in Kansas. PAC.

Jarrett, R. D. (1984). Hydraulics of high-gradient streams. *Journal of Hydraulic Engineering*, *110*(11), 1519–1539.

Johnson, J M. (2021). NHDPlus Value Added Attributes - no geometries. HydroShare. Retrieved from https://www.hydroshare.org/resource/6092c8a62fac45be97a09bfd0b0bf726/

Johnson, J. M., Afshari, S., & Rad, A. M. (2024). AHGestimation: An R package for computing robust, mass preserving hydraulic geometries and rating curves. *JOSS (in Review)*.

Johnson, J. Michael. (2022). National Hydrologic Geospatial Fabric (hydrofabric) for the Next Generation (NextGen) Hydrologic Modeling Framework. HydroShare. Retrieved from http://www.hydroshare.org/resource/129787b468aa4d55ace7b124ed27dbde

Johnson, J Michael, & Clarke, K. C. (2021). An area preserving method for improved categorical raster resampling. *Cartography and Geographic Information Science*, 1–13.

Johnson, J Michael, Coll, J. M., Ruess, P. J., & Hastings, J. T. (2018). Challenges and Opportunities for Creating Intelligent Hazard Alerts: The "FloodHippo" Prototype. *Journal of the American Water Resources Association*.

Johnson, J Michael, Munasinghe, D., Eyelade, D., & Cohen, S. (2019). An Integrated Evaluation of the National Water Model (NWM)–Height Above Nearest Drainage (HAND) Flood Mapping Methodology. *Natural Hazards and Earth System Sciences*, *19*(11), 2405–2420.

Johnson, J. Michael, Coll, J., Clarke, K. C., Afshari, S., Saksena, S., & Yeghiazarian, L. (2022). Determining Feature Based Hydraulic Geometry and Rating Curves using a Physically Based, Computationally Efficient Framework. Retrieved from https://www.preprints.org/manuscript/202212.0390

Johnson, J. Michael, Narock, T., Singh-Mohudpur, J., Fils, D., Clarke, K. C., Saksena, S., et al. (2022). Knowledge graphs to support real-time flood impact evaluation. *AI Magazine*, *43*(1), 40–45. https://doi.org/10.1002/aaai.12035

Kalyanapu, A. J., Burian, S. J., & McPherson, T. N. (2009). Effect of land use-based surface roughness on hydrologic model output. *Journal of Spatial Hydrology*, *9*(2).

Karamouz, M., & Mahani, F. F. (2021). DEM Uncertainty Based Coastal Flood Inundation Modeling Considering Water Quality Impacts. *Water Resources Management*, *35*(10), 3083–3103. https://doi.org/10.1007/s11269-021-02849-9

Kean, J. W., & Smith, J. D. (2005). Generation and verification of theoretical rating curves in the Whitewater River basin, Kansas. *Journal of Geophysical Research: Earth Surface*, *110*(F4).

Kean, J. W., & Smith, J. D. (2010). Calculation of stage-discharge relations for gravel bedded channels. *Journal of Geophysical Research: Earth Surface*, *115*(F3).

Kim, D.-H., Johnson, J. M., Clarke, K. C., & McMillan, H. K. (2024). Untangling the impacts of land cover representation and resampling in distributed hydrological model predictions. *Environmental Modelling & Software*, *172*, 105893.

Kubrak, E., Kubrak, J., Kozioł, A., Kiczko, A., & Krukowski, M. (2019). Apparent Friction Coefficient Used for Flow Calculation in Straight Compound Channels. *Water*, *11*(4), 745.

Li, Z. (2016, June). *A Framework of ArcGIS-Based Flood Inundation Modeling and Mapping System,*. Presented at the ESRI Proceedings, ESRI Proceedings. Retrieved from https://proceedings.esri.com/library/userconf/proc16/papers/265_671.pdf

Lim, N. J., Brandt, S. A., & Seipel, S. (2016). Visualisation and evaluation of flood uncertainties based on ensemble modelling. *International Journal of Geographical Information Science*, *30*(2), 240–262.

Limerinos, J. T. (1970). Determination of the Manning coefficient from measured bed roughness in natural channels.

Liu, Y. Y., Maidment, D. R., Tarboton, D. G., Zheng, X., & Wang, S. (2018). A CyberGIS Integration and Computation Framework for High-Resolution Continental-Scale Flood Inundation Mapping. *Journal of the American Water Resources Association*.

Liu, Y. Y., Tarboton, D. G., & Maidment, D. R. (2020, June 1). Height Above Nearest Drainage (HAND) and Hydraulic Property Table for CONUS - Version 0.2.1. (20200601). (Version Version 0.2.1). Oak Ridge Leadership Computing Facility. Retrieved from 10.13139/ORNLNCCS/1630903

Liu, Z., Merwade, V., & Jafarzadegan, K. (2019). Investigating the role of model structure and surface roughness in generating flood inundation extents using one-and two-dimensional hydraulic models. *Journal of Flood Risk Management*, *12*(1), e12347.

M. Foster, L., & M. Maxwell, R. (2019). Sensitivity analysis of hydraulic conductivity and Manning's n parameters lead to new method to scale effective hydraulic conductivity across model resolutions. *Hydrological Processes*, *33*(3), 332–349.

Maidment, D. R. (2016). Conceptual Framework for the National Flood Interoperability Experiment. *JAWRA Journal of the American Water Resources Association*, *53*(2), 245–257.

Mansanarez, V., Renard, B., Coz, J. L., Lang, M., & Darienzo, M. (2019). Shift Happens! Adjusting Stage-Discharge Rating Curves to Morphological Changes at Known Times. *Water Resources Research*, *55*(4), 2876–2899. https://doi.org/10.1029/2018WR023389

Marcus, W. A., Roberts, K., Harvey, L., & Tackman, G. (1992). An evaluation of methods for estimating Manning's n in small mountain streams. *Mountain Research and Development*, 227–239.

Mason, D. C., Cobby, D. M., Horritt, M. S., & Bates, P. D. (2003). Floodplain friction parameterization in two-dimensional river flood models using vegetation heights derived from airborne scanning laser altimetry. *Hydrological Processes*, *17*(9), 1711–1732.

McCormack, K. A., Levin, H. K., Morris, A. L., Fredericks, J. G., Huening, V., Tavakoly, A., et al. (2022). Validation of TDX-Hydro; a global, TanDEM-X derived, 12m resolution hydrographic data suite. In *AGU Fall Meeting Abstracts* (Vol. 2022, pp. H43B-06). Retrieved from https://ui.adsabs.harvard.edu/abs/2022AGUFM.H43B..06M/abstract

McKay, L., Bondelid, T., Dewald, T., Johnston, J., Moore, R., & Rea, A. (2012). NHDPlus Version 2: user guide. *US Environmental Protection Agency*.

McMahon, T. A., & Peel, M. C. (2019). Uncertainty in stage–discharge rating curves: application to Australian Hydrologic Reference Stations data. *Hydrological Sciences Journal*, *64*(3), 255–275.

McMillan, H., & Westerberg, I. (2015). Rating curve estimation under epistemic uncertainty. *Hydrological Processes*, *29*(7), 1873–1882.

Muste, M., Lee, K., & Bertrand-Krajewski, J.-L. (2012). Standardized uncertainty analysis for hydrometry: a review of relevant approaches and implementation examples. *Hydrological Sciences Journal*, *57*(4), 643–667.

Nguyen, H., & Fenton, J. (2005). Identification of roughness in compound channels (pp. 2512–2518). Presented at the MODSIM 2005 international congress on modelling and simulation. Modelling and Simulation Society of Australia and New Zealand.

Nobre, A. D., Cuartas, L. A., Hodnett, M., Rennó, C. D., Rodrigues, G., Silveira, A., et al. (2011). Height Above the Nearest Drainage–a hydrologically relevant new terrain model. *Journal of Hydrology*, *404*(1–2), 13–29.

Pappenberger, F., Beven, K., Horritt, M., & Blazkova, S. (2005). Uncertainty in the calibration of effective roughness parameters in HEC-RAS using inundation and downstream level observations. *Journal of Hydrology*, *302*(1–4), 46–69.

Pavelsky, T. M. (2014). Using width-based rating curves from spatially discontinuous satellite imagery to monitor river discharge. *Hydrological Processes*, *28*(6), 3035–3040.

Qi, W., & Liu, J. (2019). Studies on changes in extreme flood peaks resulting from land-use changes need to consider roughness variations. *Hydrological Sciences Journal*, *64*(16), 2015–2024. https://doi.org/10.1080/02626667.2019.1669039

Rennó, C. D., Nobre, A. D., Cuartas, L. A., Soares, J. V., Hodnett, M. G., Tomasella, J., & Waterloo, M. J. (2008). HAND, a new terrain descriptor using SRTM-DEM: Mapping terra-firme rainforest environments in Amazonia. *Remote Sensing of Environment*, *112*(9), 3469–3481.

Rojas, M., Quintero, F., & Krajewski, W. F. (2020). Performance of the national water model in iowa using independent observations. *JAWRA Journal of the American Water Resources Association*, *56*(4), 568–585.

Saksena, S., & Merwade, V. (2015). Incorporating the effect of DEM resolution and accuracy for improved flood inundation mapping. *Journal of Hydrology*, *530*, 180–194.

Schumann, G., Matgen, P., Hoffmann, L., Hostache, R., Pappenberger, F., & Pfister, L. (2007). Deriving distributed roughness values from satellite radar data for flood inundation modelling. *Journal of Hydrology*, *344*(1–2), 96–111.

Tesfa, T. K., Tarboton, D. G., Watson, D. W., Schreuders, K. A., Baker, M. E., & Wallace, R. M. (2011). Extraction of Hydrological Proximity Measures from DEMs Using Parallel Processing. *Environmental Modelling & Software*, *26*(12), 1696–1709.

Tullis, B. P. (2012). *Hydraulic loss coefficients for culverts* (Vol. 734). Transportation Research Board.

Tuozzolo, S., Langhorst, T., de Moraes Frasson, R. P., Pavelsky, T., Durand, M., & Schobelock, J. J. (2019). The impact of reach averaging Manning's equation for an in-situ dataset of water surface elevation, width, and slope. *Journal of Hydrology*, *578*, 123866.

Westerberg, I., Guerrero, J., Seibert, J., Beven, K., & Halldin, S. (2011). Stage-discharge uncertainty derived with a non-stationary rating curve in the Choluteca River, Honduras. *Hydrological Processes*, *25*(4), 603–613.

Yamazaki, D., Ikeshima, D., Sosa, J., Bates, P. D., Allen, G. H., & Pavelsky, T. M. (2019). MERIT Hydro: A High-Resolution Global Hydrography Map Based on Latest Topography Dataset. *Water Resources Research*, *55*(6), 5053–5073. https://doi.org/10.1029/2019WR024873

Yoon, Y., Beighley, E., Lee, H., Pavelsky, T., & Allen, G. (2016). Estimating flood discharges in reservoir-regulated river basins by integrating synthetic SWOT satellite observations and hydrologic modeling. *Journal of Hydrologic Engineering*, *21*(4), 05015030.

Zheng, X., Tarboton, D. G., Maidment, D. R., Liu, Y. Y., & Passalacqua, P. (2017). River channel geometry and rating curve estimation using height above the nearest drainage. *Journal of the American Water Resources Association*.

Zheng, X., Maidment, D. R., Tarboton, D. G., Liu, Y. Y., & Passalacqua, P. (2018). GeoFlood: Large-Scale Flood Inundation Mapping Based on High-Resolution Terrain Analysis. *Water Resources Research*.